Available online at www.sciencedirect.com
ScienceDirect
Journal of Sound and Vibration 324 (2009) 608–621
JOURNAL OF SOUND AND VIBRATION
www.elsevier.com/locate/jsvi

Modeling and characterization of a bimorph impedance transducer

Hou Xiaoyan*

Department of Civil Engineering, National University of Singapore, Singapore 117576, Singapore

Received 17 February 2009; accepted 28 February 2009
Handling Editor: L.G. Tham
Available online 5 April 2009

Abstract

In this paper, a bimorph impedance transducer (BIT), which is utilized as a simultaneous actuator and sensor for mechanical impedance measurement, is modeled and analytically characterized. A four-pole model is constructed to correlate the desired translational mechanical impedance with the measured electrical impedance. From the four-pole model, two set functions are defined to describe the system dynamics of the transducer. Closed-form expressions for these functions are then derived based on piezoelectric constitutive equations and beam theory. Besides producing accurate predications, as verified by a series of experiments, the analytical studies provide strong physical insight into the interaction between the transducer and the external load applied to it. Through two examples, it is found that the analytical solutions are also useful in improving the actuation efficiency and sensing capability of a BIT.

1. Introduction

As bending bimorphs possess high motion and voltage sensitivity, they are widely used as electromechanical transducers, such as accelerometers [1], resonators [2], laser beam deflectors [3], air acoustic transducers [4], microscopes [5], and pumps [6]. Due to the extensive applications, a lot of researchers have tried to analytically model bending bimorphs. The two most widely used approaches are admittance matrix approach and equivalent circuit approach.

Admittance matrix approach is extensively adopted in modeling bimorph transducers as it describes the electromechanical coupling in a bimorph. In 1991, Smits et al. developed the linear constituent relations of a cantilever bimorph for static case [7]. Their paper was a milestone in characterizing the electromechanical properties of bending bimorph. In their work, the bimorph was put in a constant electrical field. One end of the bimorph was fixed without displacement, the other end was free and subjected to different kind of load (moment, force, or uniformly distributed pressure). Using the internal energy method by assuming thermodynamic quasi-equilibrium, the cantilever bimorph under various constant mechanical/electrical loads was characterized by a 4×4 matrix equation.

*Tel.: +86 13120938530.
E-mail address: houxiaoyan@gmail.com

0022-460X/$ - see front matter © 2009 Elsevier Ltd. All rights reserved.
doi:10.1016/j.jsv.2009.02.050

In order to get a better understanding of the bimorph behavior as a function of frequency, Smits et al. developed a dynamic admittance matrix for cantilever bimorph which related the harmonically varying diving parameters to their response parameters [8,9]. Through evaluating the dynamic performance of the bimorph under external excitations, the elements in the dynamic admittance matrix were identified analytically.

As piezoelectric bimorphs are widely used in industrial equipment, it is useful to cast the bimorph constituent equations in network representation [10]. In this way, bimorph sensors or actuators can be fully and rapidly incorporated into the world of electronics. Cho et al. proposed an important equivalent circuit model in 2000 [11]. In their studies, a 5×5 impedance matrix was determined to describe the dynamic behavior of a bimorph beam. The extensive parameters considered are forces and moments at both ends of the bimorph and electrical voltage across the bimorph. Cho's model is feasible for bimorphs with various end conditions. However, like other equivalent circuit models, Cho's model is complex. For different end conditions or external mechanical loads, complicated circuits have to be developed and then simplified to get the results.

In the past decades, though a lot of researchers have investigated the performance of piezoelectric bimorph as a sensor or an actuator, little research work was done in using bimorph as a sensor and an actuator simultaneously. In this paper, based on a Sensor cum Actuator (SCA) technique [12,13], a Bimorph Impedance Transducer (BIT), in which two bimorphs serve as the essential actuating and sensing elements for translational mechanical impedance measurement, will be studied. After modeling the BIT using a four-pole model, the transducer is calibrated analytically. Closed-form calibration functions and transduction functions, which describe the system dynamics of the transducer, will be derived in conjunction with piezoelectric constitutive equations and beam theory. Besides providing strong physical insight into the interaction between the transducer and the external load applied to it, the analytical solutions produce accurate predictions of the amplitude of the functions, as will be verified by experiments. Using the closed-form formulae, the actuation efficiency and sensing capability of a BIT will be further investigated through changing the material and geometric parameters of the BIT.

2. Working principles of the BIT for translational impedance measurement

The BIT contains two series type bimorphs, an insulating layer and a rigid supporting block, as shown in Fig. 1. The two bimorphs have identical geometric and material characteristics and are symmetrically attached to the glass epoxide layer, which effectively prevents the charge convection between the left and right bimorphs. The bottom of the insulating layer is tightly glued to the supporting block, which is made of aluminum and has a dimension of $15\,\text{mm} \times 15\,\text{mm} \times 15.8\,\text{mm}$. As illustrated in Fig. 1, x-axis is along the bimorph length direction, y-axis along the bimorph width direction and z-axis along the thickness direction.

When ac voltages of same amplitude and phase are supplied to the left and right bimorphs, the bimorphs are set into bending vibrations synchronously (Fig. 2). Dynamic forces and moments are generated at the connecting parts between the bimorphs and the insulating layer due to the inverse piezoelectric effect. As the transducer is symmetric (though during fabrication, slight difference exists), the moments have the same amplitude but opposite direction, therefore they cancel out each other; while, the dynamic forces are identical in both amplitude and direction, thus they are doubled in magnitude and exerted to the test structure through

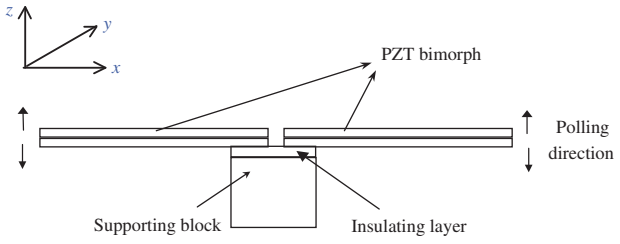

Fig. 1. Structure of the bimorph impedance transducer.

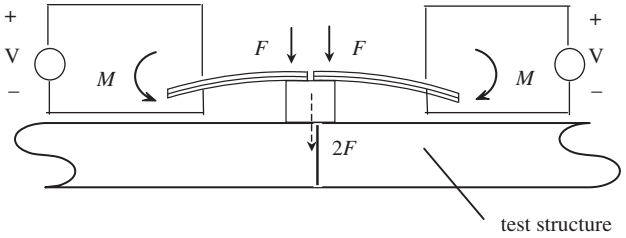

Fig. 2. Working principles of the BIT for translational impedance measurement.

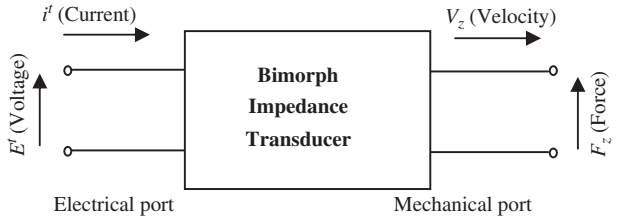

Fig. 3. Translational four-pole model of the bimorph impedance transducer.

the supporting block. At the same time of actuation, the response of the structure affects the motion of the transducer due to the direct piezoelectric effect. To describe the simultaneous actuation/sensing process, a translational two-port model is constructed as shown in Fig. 3. A matrix equation correlates the voltage and current at the electrical port with the force and velocity at the mechanical port of the BIT:

$$\begin{bmatrix} V^t \\ i^t \end{bmatrix} = \begin{bmatrix} a_{11} & a_{12} \\ a_{21} & a_{22} \end{bmatrix} \cdot \begin{bmatrix} F_z \\ v_z \end{bmatrix} \tag{1}$$

where V^t is the electrical voltage applied to the left and right bimorphs, i^t is the sum of the electrical current on the bimorphs, and F_z and v_z are the output force and velocity along z-direction.

The 2×2 matrix in Eq. (1) describes the dynamic characteristics of the BIT for translational measurement. The four elements in the matrix are called transduction functions. They are normally frequency spectra describing the relationships between one input electrical variable and one output mechanical variable.

$$a_{11} = V^t/F_z|_{vz=0} \tag{2}$$

$$a_{21} = i^t/F_z|_{vz=0} \tag{3}$$

$$a_{12} = V^t/v_z|_{Fz=0} \tag{4}$$

$$a_{22} = i^t/v_z|_{Fz=0} \tag{5}$$

The translational mechanical impedance of the host structure at the excitation point can be expressed as

$$Z_z^t = \frac{F_z}{v_z} \tag{6}$$

The input electrical impedance of the transducer is

$$Z_e^t = \frac{V^t}{i^t} \tag{7}$$

Combining Eqs. (1)–(7), we have

$$Z_z^t = -\frac{a_{22}Z_e^t - a_{12}}{a_{21}Z_e^t - a_{11}} \tag{8}$$

As shown in Eq. (8), after calibration functions a_{11}, a_{21}, a_{12}, and a_{22} are made available, translational mechanical impedance at the measurement point can be evaluated from the input electrical impedance. However, in experiments, these functions are difficult to measure using conventional transducers. The loading effects of conventional load cells and accelerometers for force and acceleration measurement are too big to ignore due to the small size and low weight of the BIT. To avoid these difficulties, an alternative calibration method was developed to characterize the BIT.

In Eq. (1), if letting i^t, F_z, and v_z equal to zero, respectively, we have another set of calibration functions:

$$Z^t_{MO} = \left.\frac{F_z}{v_z}\right|_{it=0} \tag{9}$$

$$Z^t_{ef} = \left.\frac{V^t}{i^t}\right|_{Fz=0} \tag{10}$$

$$Z^t_{ec} = \left.\frac{V^t}{i^t}\right|_{vz=0} \tag{11}$$

where Z^t_{MO} is the translational impedance of the BIT when it is electrically open-circuited, Z^t_{ef} and Z^t_{ec} are the electrical impedances of the transducer when it is freely suspended and clamped onto the ground, respectively.

Combining Eqs. (1)–(11), the translational impedance at the excitation point is

$$Z^t_z = Z^t_{MO}\frac{Z^t_e - Z^t_{ef}}{Z^t_e - Z^t_{ec}} \tag{12}$$

As discussed above, two sets of functions could be utilized to describe the system dynamics of the BIT: transduction functions (a_{11}, a_{12}, a_{21}, a_{22}) and calibration functions ($Z^t_{MO}, Z^t_{ef}, Z^t_{ec}$). To gain further insight into the newly designed BIT, the relationship between these functions and the material and geometric properties of the BIT are described in the following paragraphs.

3. Analytical calibration

The left and right piezoelectric bimorphs in the prototype BIT come from Fuji Ceramics C-6 series and have dimensions of 63 mm × 15 mm × 1 mm. Table 1 lists their material properties and dimensions. In the following analysis, as the BIT is designed to be symmetric about x-axis, only one half of the transducer with symmetric boundary condition will be studied.

3.1. Motion equation of a bimorph in the BIT

According to piezoelectric constitutive equations, the electromechanical coupling of the bimorph in Fig. 1 can be expressed as

$$\text{For upper PZT}: \ S^p_1 = s^E_{11}T^p_1 - d_{31}E_3 \tag{13}$$

$$D_3 = -d_{31}T^p_1 + \varepsilon^T_{33}E_3 \tag{14}$$

$$\text{For lower PZT}: \ S^p_1 = s^E_{11}T^p_1 + d_{31}E_3 \tag{15}$$

$$D_3 = d_{31}T^p_1 + \varepsilon^T_{33}E_3 \tag{16}$$

where S^p_1 and T^p_1 are the strain and stress of the PZT layers parallel with x-axis, E_3 and D_3 are the electric field and dielectric displacement along z-direction, s^E_{11} is the mechanical compliance under constant electric field condition, d_{31} is the piezoelectric constant, and ε^T_{33} is the permittivity under constant stress condition.

Table 1
Material and geometric properties of the bimorphs in the prototype BIT.

	Unit	Nomenclature	
Piezoelectric elements			
Density	kg/m^3	ρ	7400
Poisson's ratio		σ^E	0.31
Elastic modulus (*e* formal)	$\times 10^{10}\,N/m^2$	C_{11}^E	12.3
		C_{12}^E	7.7
		C_{13}^E	8.0
		C_{33}^E	11.2
		C_{44}^E	1.9
		C_{66}^E	2.3
Piezoelectric constants	C/m^2	e_{31}	−7.3
		e_{33}	17.2
		e_{15}	14.5
Relative dielectric constants		$\varepsilon_{11}^S/\varepsilon_0$	1039
		$\varepsilon_{33}^S/\varepsilon_0$	749
Coupling factors	$\times 10^{-2}$	K_{31}	40.9
Mechanical Q		Q_m	82
Length	m	l_{total}	0.063
Cantilevered length	m	l	0.05655
Width	m	b	0.015
Thickness	m	$2h_p$	0.0009
Middle metal layer			
Elastic constant	m^2/N	s_{11}^m	8.9286×10^{-12}
Density	kg/m^3	ρ	8800
Thickness	m	$2h_m$	0.0001

For the middle metal layer, from Hook's law, we have

$$S_1^m = s_{11}^m T_1^m \tag{17}$$

where T_1^m and S_1^m are the stress and strain of the metal layer and s_{11}^m the mechanical compliance of the metal.

Assuming the bimorph undergoes small deflections in the linearly elastic region, it is viewed as a Euler–Bernoulli beam. A small bimorph element is depicted in Fig. 4. w is the out-of-plane displacement of the bimorph's neutral plane from its unloaded position to its loaded position. This displacement is usually accompanied by the rotation of the neutral plane:

$$\alpha = -\frac{\mathrm{d}w}{\mathrm{d}x} \tag{18}$$

The strains in the PZT element and the metal layer are

$$S_1^p = \frac{\mathrm{d}u^p}{\mathrm{d}x} = \frac{\mathrm{d}\alpha}{\mathrm{d}x} z^p \quad \text{and} \quad S_1^m = \frac{\mathrm{d}u^m}{\mathrm{d}x} = \frac{\mathrm{d}\alpha}{\mathrm{d}x} z^m \tag{19}$$

where z^p and z^m are the z-coordinate of a thin PZT layer and a metal layer, respectively, and u^p and u^m are the corresponding transverse displacement.

For the bimorph element in Fig. 4, direct stresses T_1^p and T_1^m create moments about the neutral plane. Summing these moments over the cross-section area results in a total bending moment:

$$M_y = \int\int z^p T_1^p \,\mathrm{d}y\,\mathrm{d}z + \int\int z^m T_1^m \,\mathrm{d}y\,\mathrm{d}z \tag{20}$$

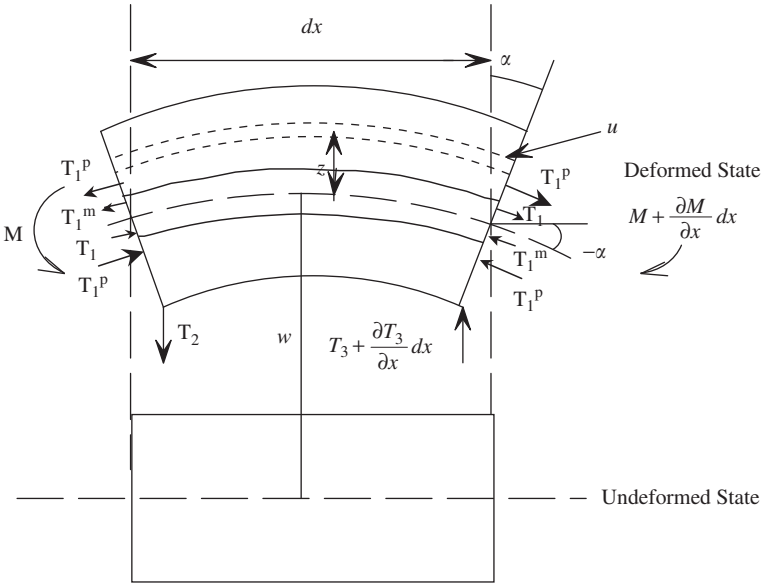

Fig. 4. Diagram of a small bimorph element.

When summing the shear stresses T_3^p and T_3^m, the total shear force becomes

$$F_3 = F_3^p + F_3^m = \int\int T_3^p \,\mathrm{d}y\,\mathrm{d}z + \int\int T_3^m \,\mathrm{d}y\,\mathrm{d}z \tag{21}$$

Consider the moment equilibrium of the bimorph element, we have

$$M_y + \frac{\partial M_y}{\partial x}\,\mathrm{d}x - M_y - F_3\,\mathrm{d}x = 0 \rightarrow F_3 = \frac{\mathrm{d}M_y}{\mathrm{d}x} \tag{22}$$

Taking advantages of Eqs. (13)–(17),

$$M_y = -\frac{2b}{3}\left\{\frac{1}{s_{11}^E}[(h_p+h_m)^3 - h_m^3] + \frac{1}{s_{11}^m}h_m^3\right\}\frac{\mathrm{d}^2w}{\mathrm{d}x^2} - \frac{d_{31}b}{2s_{11}^E}(h_p+2h_m)V \tag{23}$$

$$F_3 = \frac{\mathrm{d}M}{\mathrm{d}x} = -\frac{2b}{3}\left\{\frac{1}{s_{11}^E}[(h_p+h_m)^3 - h_m^3] + \frac{h_m^3}{s_{11}^m}\right\}\frac{\mathrm{d}^3w}{\mathrm{d}x^3} \tag{24}$$

where b and h_p are the width and thickness of one PZT layer, $2h_m$ is the thickness of the middle metal layer, and V is the excitation voltage.

Applying Newton's second law to the bimorph element in z-direction yields:

$$\sum F_z = ma_z = (2\rho_m h_m b\,\mathrm{d}x + 2\rho_p h_p b\,\mathrm{d}x)\frac{\partial^2 w}{\partial t^2} = F_3 + \frac{\partial F_3}{\partial x}\,\mathrm{d}x - F_3$$

$$2b(\rho_m h_m + \rho_p h_p)\frac{\partial^2 w}{\partial t^2} = \frac{\partial F_3}{\partial x} = \frac{\partial^2 M_y}{\partial x^2} \tag{25}$$

Substituting Eq. (23) into Eq. (25), the motion equation which governs the transverse motion of the bimorph is obtained as

$$-\frac{2b}{3}\left\{\frac{1}{s_{11}^E}[(h_p+h_m)^3 - h_m^3] + \frac{h_m^3}{s_{11}^m}\right\}\frac{\partial^4 w}{\partial x^4} + 2b(\rho_m h_m + \rho_p h_p)\frac{\partial^2 w}{\partial t^2} = 0 \tag{26}$$

where ρ_p and ρ_m are the densities of the PZT and the metal layers.

3.2. Identification of transduction functions and calibration functions

As shown in Eq. (26), the out-of-plane displacement w is a function of both the x coordinate and time. Through separating variables, the general solution for the harmonic vibration in Eq. (26) is obtained as

$$w = [k_1 \cos(\Omega x) + k_2 \sin(\Omega x) + k_3 \cosh(\Omega x) + k_4 \sinh(\Omega x)]\, e^{j\omega t} \tag{27}$$

where

$$\Omega = \sqrt[4]{\frac{2b(\rho_p h_p + \rho_m h_m)\omega^2}{\frac{2b}{3}\left\{\frac{1}{s_{11}^E}[(h_p + h_m)^3 - h_m^3] + \frac{h_m^3}{s_{11}^m}\right\}}}$$

Since the BIT is driven by sinusoidal voltage, the assumption of the harmonic time dependence $e^{j\omega t}$ is justified.

From Eq. (27), we have the expressions for rotation, bending moment, and shear force, which are functions of the four coefficients k_1, k_2, k_3, k_4:

$$\alpha = -\Omega[-k_1 \sin(\Omega x) + k_2 \cos(\Omega x) + k_3 \sinh(\Omega x) + k_4 \cosh(\Omega x)] \tag{28}$$

$$M_y = -\frac{2\Omega^2 b}{3}\left[\frac{(h_p + h_m)^3 - h_m^3}{s_{11}^E} + \frac{h_m^3}{s_{11}^m}\right][-k_1 \cos(\Omega x) - k_2 \sin(\Omega x) + k_3 \cosh(\Omega x) + k_4 \sinh(\Omega x)] - \frac{d_{31} b}{2 s_{11}^E}(h_p + 2h_m)V \tag{29}$$

$$F_3 = -\frac{2\Omega^3 b}{3}\left[\frac{(h_p + h_m)^3 - h_m^3}{s_{11}^E} + \frac{h_m^3}{s_{11}^m}\right][k_1 \sin(\Omega x) - k_2 \cos(\Omega x) + k_3 \sinh(\Omega x) + k_4 \cosh(\Omega x)] \tag{30}$$

In the frequency domain, the electrical current on the bimorph is

$$I = b d_{31} \int_0^l \frac{dT_1^p}{dt}\, dx + \frac{j\omega b l}{2h_p}\left(\varepsilon_{33}^T - \frac{d_{31}^2}{s_{11}^E}\right)V \tag{31}$$

Now with these expressions, calibration functions ($Z_{ec}^t, Z_{ef}^t, Z_{MO}^t$) and transduction functions ($a_{11}, a_{21}, a_{12}, a_{22}$) can be determined under different boundary conditions. First, for Z_{ec}^t, a_{11}, and a_{21}, mechanically clamped condition is considered. Under clamped condition, as the stiffness of the supporting block in the z-direction is much higher than that of the bimorph, the supporting block is treated as a rigid body. The displacement constraints at the bottom of the block are therefore tantamount to the constraints at the connecting part between the block and the bimorph. The other end of the bimorph is totally free. Above boundary conditions lead to the following equations:

$$F_{3A} = 0 \quad M_{yA} = 0$$

$$w_B = 0 \quad \alpha_B = 0$$

Solving above equations, we have the closed-form formulae for Z_{ec}^t, a_{11}, and a_{21}:

$$Z_{ec} = \frac{1}{j\omega\left[\frac{3d_{31}^2 b(h_p + h_m)^2}{8\Omega s_{11}^{E^2}\left\{\frac{1}{s_{11}^E}[(h_p + h_m)^3 - h_m^3] + \frac{h_m^3}{s_{11}^m}\right\}}\frac{\sinh(\Omega l)\cos(\Omega l) + \sin(\Omega l)\cosh(\Omega l)}{1 + \cos(\Omega l)\cosh(\Omega l)} + \frac{bl}{2h_p}\left(\varepsilon_{33}^T - \frac{d_{31}^2}{s_{11}^E}\right)\right]} \tag{32}$$

$$a_{11} = \frac{2 s_{11}^E}{d_{31} b \Omega (h_p + 2h_m)}\frac{1 + \cos(\Omega l)\cosh(\Omega l)}{\sin(\Omega l) - \sinh(\Omega l)} \tag{33}$$

$$a_{21}=\frac{2s_{11}^E}{\mathrm{j}\omega d_{31}b\Omega(h_p+2h_m)}\frac{1+\cos(\Omega l)\,\cosh(\Omega l)}{\sin(\Omega l)-\sinh(\Omega l)}$$
$$\times\left[\frac{3d_{31}^2b(h_p+h_m)^2[\sinh(\Omega l)\,\cos(\Omega l)+\sin(\Omega l)\cosh(\Omega l)]}{8\Omega s_{11}^E\left\{\frac{1}{s_{11}^E}[(h_p+h_m)^3-h_m^3]+\frac{h_m^3}{s_{11}^m}\right\}[1+\cos(\Omega l)\,\cosh(\Omega l)]}+\frac{bl}{2h_p}\left(\varepsilon_{33}^T-\frac{d_{31}^2}{s_{11}^E}\right)\right] \tag{34}$$

Mechanically free condition is then applied to the BIT to identify Z_{ef}^t, a_{12}, and a_{22}. According to the definitions in Eqs. (4), (5), and (10), identical voltages supplied to the bimorphs of the BIT result in the translational vibrations of the output port of the transducer (the bottom of the supporting block) along the z-direction while rotation is inhibited. In this situation, the supporting block is treated as a concentrated mass. As a result, an inertial force caused by the vibrations of the block is loaded to the right end of the bimorph. The left end of the bimorph is free. These boundary conditions lead to:

$$F_{3A}=0\quad M_{yA}=0$$

$$F_{3B}=-m\omega^2w_B\quad \alpha_B=0$$

Combining above equations with Eqs. (27)–(31), we have the closed-form expressions for Z_{ef}^t, a_{12}, and a_{22}:

$$Z_{ef}=\frac{1}{\mathrm{j}\omega\left[\frac{3d_{31}^2b(h_p+h_m)^2}{8\Omega s_{11}^{E^2}\left\{\frac{1}{s_{11}^E}[(h_p+h_m)^3-h_m^3]+\frac{h_m^3}{s_{11}^m}\right\}}A+\frac{bl}{2h_p}\left(\varepsilon_{33}^T-\frac{d_{31}^2}{s_{11}^E}\right)\right]} \tag{35}$$

$$a_{12}=\frac{4\Omega^2s_{11}^E\left\{\frac{1}{s_{11}^E}[(h_p+h_m)^3-h_m^3]+\frac{h_m^3}{s_{11}^m}\right\}}{3\mathrm{j}\omega\gamma d_{31}(h_p+2h_m)}C \tag{36}$$

$$a_{22}=\frac{4C\Omega^2s_{11}^E\left\{\frac{1}{s_{11}^E}[(h_p+h_m)^3-h_m^3]+\frac{h_m^3}{s_{11}^m}\right\}}{3\gamma d_{31}(h_p+2h_m)}$$
$$\times\left[\frac{3Ad_{31}^2b(h_p+h_m)^2}{8\Omega s_{11}^{E^2}\left\{\frac{1}{s_{11}^E}[(h_p+h_m)^3-h_m^3]+\frac{h_m^3}{s_{11}^m}\right\}}+\frac{bl}{2h_p}\left(\varepsilon_{33}^T-\frac{d_{31}^2}{s_{11}^E}\right)\right] \tag{37}$$

where

$$\gamma=\frac{2b\Omega^3\left\{\frac{1}{s_{11}^E}[(h_p+h_m)^3-h_m^3]+\frac{h_m^3}{s_{11}^m}\right\}}{3m\omega^2}$$

$$A=\frac{\cos(\Omega l)\,\sinh(\Omega l)+\sin(\Omega l)\,\cosh(\Omega l)+2\gamma\,\sin(\Omega l)\,\sinh(\Omega l)}{1+\cos(\Omega l)\,\cosh(\Omega l)+\gamma\,\sin(\Omega l)\,\cosh(\Omega l)+\gamma\,\cos(\Omega l)\,\sinh(\Omega l)}$$

$$C=\frac{1+\cos(\Omega l)\,\cosh(\Omega l)+\gamma\,\sin(\Omega l)\,\cosh(\Omega l)+\gamma\,\cos(\Omega l)\,\sinh(\Omega l)}{\sinh(\Omega l)-\sin(\Omega l)}$$

$2m=$ mass of the supporting block.

From Eq. (12), besides Z^t_{ec} and Z^t_{ef}, Z^t_{MO} is another indispensable calibration function defining the system dynamics of the BIT. Its analytical formula is derived from transduction functions a_{21} and a_{22} by

$$Z^t_{MO} = \left.\frac{F_z}{v_z}\right|_{it=0} = -\frac{a_{22}}{a_{21}}$$

$$= -\frac{2C\Omega^3 j\omega b\left\{\frac{1}{s^E_{11}}[(h_p+h_m)^3 - h_m^3] + \frac{h_m^3}{s^m_{11}}\right\}\left[\frac{3Ad^2_{31}b(h_p+h_m)^2}{8\Omega s^{E^2}_{11}\left\{\frac{1}{s^E_{11}}[(h_p+h_m)^3 - h_m^3] + \frac{h_m^3}{s^m_{11}}\right\}} + \frac{bl}{2h_p}\left(\varepsilon^T_{33} - \frac{d^2_{31}}{s^E_{11}}\right)\right]}{\frac{3\gamma[1+\cos(\Omega l)\cosh(\Omega l)]}{\sin(\Omega l) - \sinh(\Omega l)}\left[\frac{3d^2_{31}b(h_p+h_m)^2[\sinh(\Omega l)\cos(\Omega l) + \sin(\Omega l)\cosh(\Omega l)]}{8\Omega s^E_{11}\left\{\frac{1}{s^E_{11}}[(h_p+h_m)^3 - h_m^3] + \frac{h_m^3}{s^m_{11}}\right\}[1+\cos(\Omega l)\cosh(\Omega l)]} + \frac{bl}{2h_p}\left(\varepsilon^T_{33} - \frac{d^2_{31}}{s^E_{11}}\right)\right]} \tag{38}$$

Based on the above discussions, it is concluded that calibration functions ($Z^t_{ec}, Z^t_{ef}, Z^t_{MO}$) and transduction functions (a_{11}, a_{21}, a_{12}, a_{22}) are frequency spectra solely depending on the actuating frequency and the material and geometric characteristics of the transducer itself. For the prototype transducer with properties listed in Table 1, these functions are calculated using the formulae in Eqs. (32)–(38), as depicted in Figs. 5 and 6. As BIT is a light-damped structure, here when analytically calibrating it, damping is not taken into account as in above analysis, here only amplitude information is obtained.

4. Experimental verifications

In this section, experiments were carried out to validate the formulae derived in the last section. As transduction functions (a_{11}, a_{21}, a_{12}, a_{22}) are difficult to measure as discussed in Section 2, only calibration functions ($Z^t_{ec}, Z^t_{ef}, Z^t_{MO}$) were experimentally evaluated.

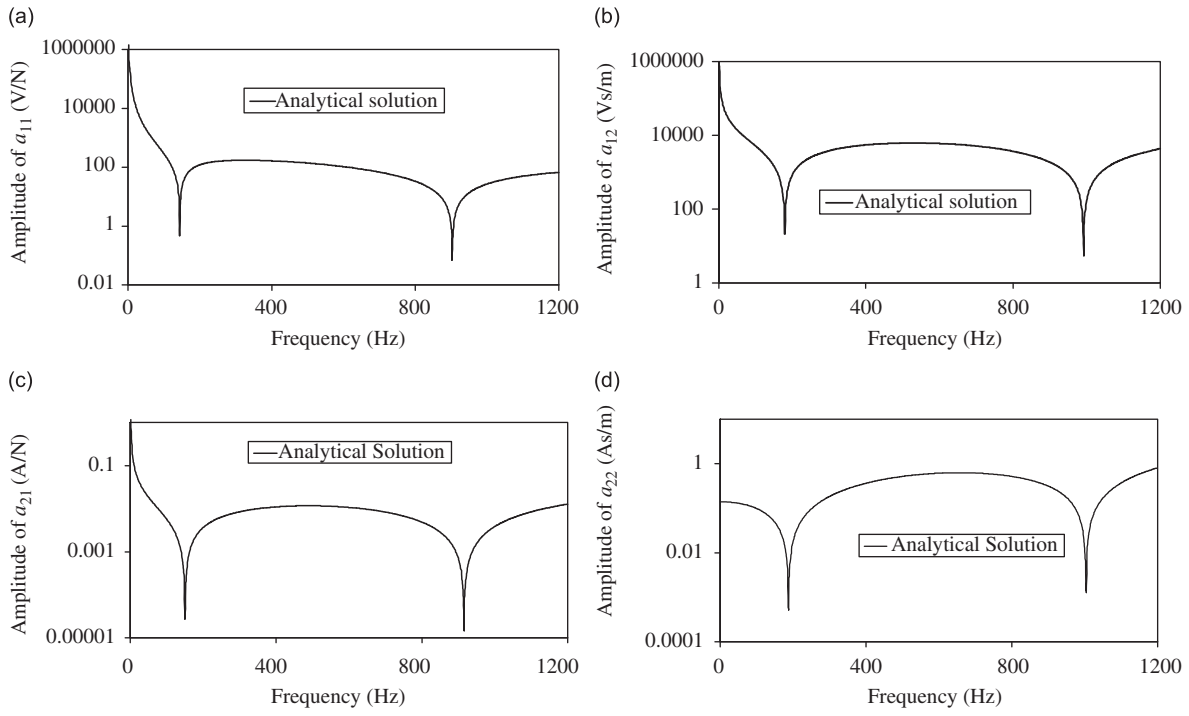

Fig. 5. Analytically calculated transduction functions (a) a_{11}, (b) a_{12}, (c) a_{21}, and (d) a_{22}.

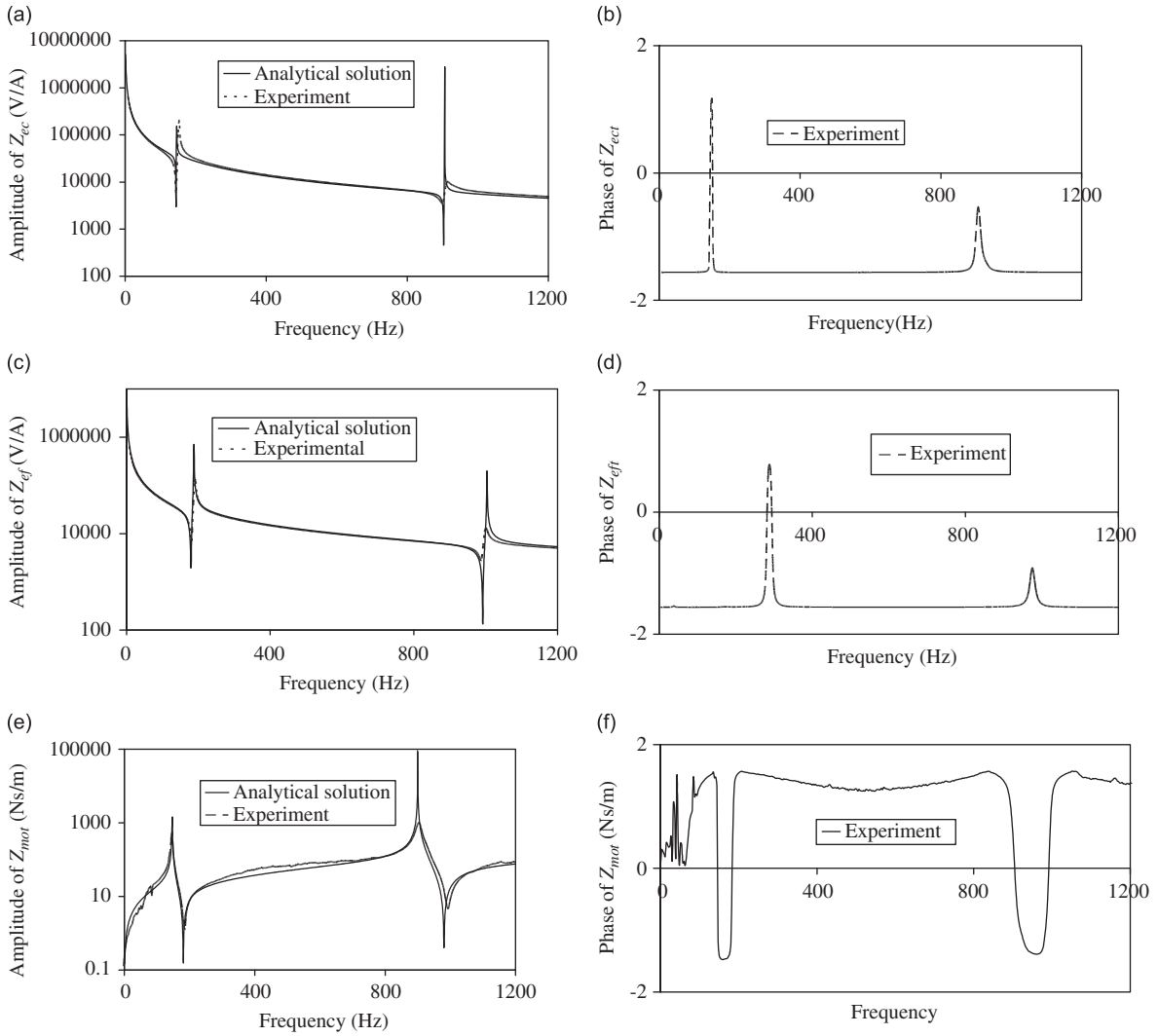

Fig. 6. Comparison of calibration functions between analytical and experimental results: (a) amplitude of Z^t_{ec}, (b) phase of Z^t_{ec}, (c) amplitude of Z^t_{ef}, (d) phase of Z^t_{ef}, (e) amplitude of Z^t_{MO}, and (f) phase of Z^t_{MO}.

To identify Z^t_{ec} and Z^t_{ef}, mechanically clamed and free conditions were achieved, respectively. The clamped boundary condition was realized by clamping BIT (0.024 kg) onto an 18 kg base (Fig. 7(a)). The free condition was performed by suspending the transducer with an elastic string, as shown in Fig. 7(b). Since the natural frequency of the suspended system is far below the frequency range of interest, the effect of the string on measurement can be ignored.

Under both clamped and free conditions, identical voltage excitations in the form of a sine sweep were generated by an SI 1260 Impedance/Gain-Phase Analyzer and supplied to the left and right bimorphs of the BIT. The input electrical impedance was simultaneously measured by the analyzer. The measured Z^t_{ec} and Z^t_{ef} versus frequency are compared with the analytical solutions in Fig. 6.

For another calibration function Z^t_{MO}, due to the fact that BIT is small and light, it is almost impossible to directly measure Z^t_{MO} using conventional sensors. In experiments, instead of directly measuring force and velocity, an alternative identification method was adopted, in which a series of rigid cuboids with known masses were loaded to the BIT one by one, serving as a known mechanical load (Fig. 7(c)). As the cuboid can be treated as an ideal rigid body with mass m, its translational mechanical impedance at any frequency is

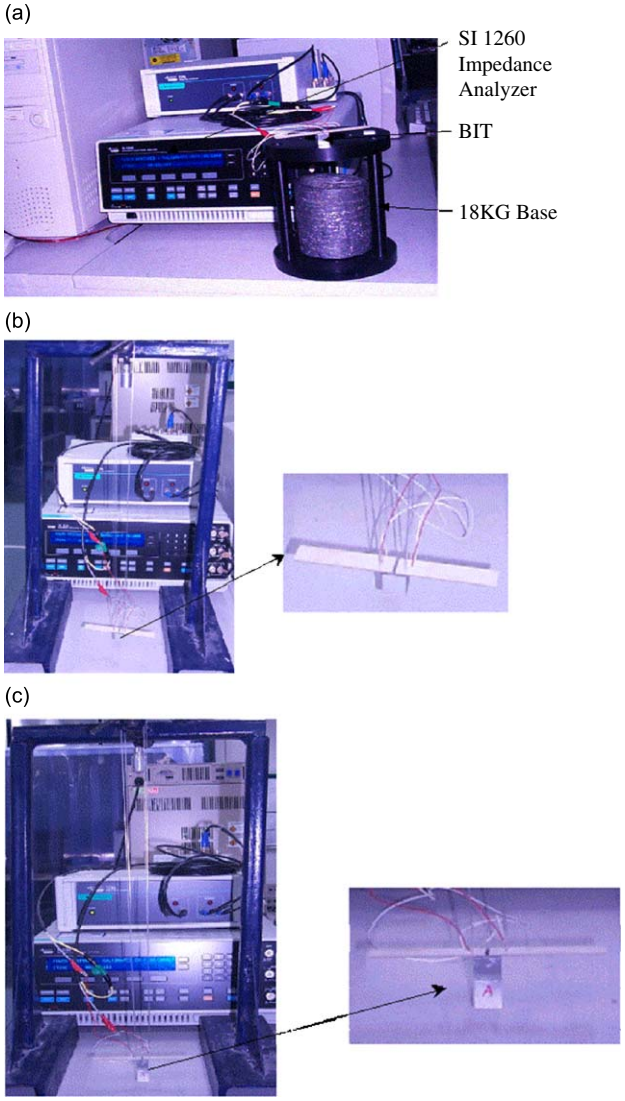

Fig. 7. Experimental setup to identify calibration functions Z^t_{ec}, Z^t_{ef}, Z^t_{MO}: (a) measurement of Z^t_{ec}, (b) measurement of Z^t_{ef}, and (c) measurement of Z^t_{MO}.

known as

$$Z^t_z = \frac{F_z}{v_z} = \frac{ma_z}{v_z} = \frac{m}{v_z}\omega v_z = m\omega = 2\pi f \mathrm{j} m \tag{39}$$

For each cuboid, taking advantages of Z^t_{ec} and Z^t_{ef}, which have been experimentally determined above, Z^t_{MO} can be determined from the measured Z^t_e:

$$Z^t_{MO} = \frac{F_z}{v_z} = 2m\pi f \mathrm{j}\frac{Z_e - Z_{ec}}{Z_e - Z_{ef}} \tag{40}$$

To minimize measurement errors, eight calibration masses were employed to experimentally determine Z^t_{MO}: 3.65, 4.85, 5.60, 6.09, 7.04, 9.09, 10.92, and 16.64 g. For each mass, testing illustrated in Fig. 7(c) was carried out. A calibration mass was glued to the supporting block of the transducer; the transducer and calibration mass system was freely suspended with elastic string. After ac voltage of same amplitude and phase was

supplied to the left and right bimorphs, the electrical impedance Z_e^t was measured using the SI Impedance Analyzer. Then averaging process was performed to get the final results (Fig. 6).

When comparing the experimental and analytical data for Z_{ec}^t and Z_{ef}^t in Fig. 6(a) and (c), it can be seen that the amplitude curves from experiments and analytical calculations agree very well over the whole frequency range up to 1200 Hz. However, since damping is not included in the analytical solutions, as expected, the amplitudes from analytical formulae are larger than those from experiments at resonances and anti-resonances. For Z_{MO}^t in Fig. 6(e), it is observed that Z_{MO}^t determined via the two calibration ways (analytical and experimental) are comparable. The discrepancy is greater at the low frequency range. This may be accounted for by the fact that in the low frequency range, the amplitude of Z_e^t is quite big as the current is small and is similar with those of Z_{ec}^t and Z_{ef}^t, therefore errors are more liable to occur according to Eq. (40). The difference among the experimental and analytical results is also due to the fact that the analytical studies were based on ideal conditions; while, in experiments, the fabrication of the BIT and the rigid masses was not absolutely ideal. Even so, the confirmation of the theoretical prediction by the experimental results is good.

5. Improvement of the SCA performance of a BIT

A conventional sensor is desired to be as small as possible to achieve high measurement accuracy. In contrast, a conventional actuator should be as large as possible to minimize its effect on measurement. While, for the BIT, which serves as a sensor and an actuator simultaneously, until now, there has not been a well-accepted criterion defining its optimal SCA performance. However, it is safe to say that a "good" BIT should have high actuation efficiency to effectively excite the tested structure and high sensing capability to detect even small variations in the measurand.

Since a BIT performs actuating during measurement, it is necessary to discuss its actuation efficiency. According to the definitions in Eqs. (2) and (4), a_{11} describes the relationship between the excitation voltage and the output force under clamped condition; a_{12} defines the relationship between the voltage and the linear velocity under free condition. As a BIT is driven by voltage, an examination of a_{11} and a_{12} provides us information on the actuation efficiency of a BIT. To improve actuating efficiency, amplitudes of a_{11} and a_{12} are preferred to be as small as possible at a given excitation frequency so that BIT produces higher output force or velocity for any given excitation voltages.

As BIT also performs sensing, it is desired that the measurand, namely, the input electrical impedance Z_e^t, is accurately detected. Z_{ec}^t and Z_{ef}^t are the electrical impedances of BIT corresponding to two extreme boundary conditions: clamped and free conditions. Any test structure, which serves as a mechanical load to the transducer, falls between these two conditions. Therefore, an examination of Z_{ec}^t and Z_{ef}^t will give us some information on the sensing ability of a BIT.

In Section 3, the closed-form calibration functions ($Z_{ec}^t, Z_{ef}^t, Z_{MO}^t$) and transduction functions (a_{11}, a_{12}, a_{21}, a_{22}) have been analytically derived. Taking advantages of these formulae, it is possible to improve the SCA performance of a BIT through studying the influence of its essential design parameters on its dynamic performance. In this paper, two cases are considered as examples. In the first case, the electrical connection type of the bimorphs in a BIT is changed from the series type as in the prototype transducer to the parallel type. This change introduces additional factors in Eqs. (13)–(16): the piezoelectric coefficient d_{31} is multiplied by two and the dielectric term ε_{33}^T is multiplied by four [14]. In the second case, the material properties are kept unchanged, while the thickness of the bimorphs changed from 0.35 mm, 0.45 mm, to 0.55 mm. In both cases, transduction functions a_{11} and a_{12} as well as calibration functions Z_{ec}^t and Z_{ef}^t are calculated using Eqs. (33), (36), (32), and (35). The amplitudes of these functions versus frequency are depicted in Figs. 8 and 9, respectively.

As shown in Fig. 8, the changes in the piezoelectric coefficient and the dielectric term do not alter the natural frequencies of the four functions studied. However, it has significant influence in the amplitudes of all the functions. At any frequency, for a given excitation voltage, the output force or velocity is doubled for the clamped or free boundary condition, and the electrical impedances Z_{ec}^t and Z_{ef}^t become only one-fourth of the original values. It is therefore concluded that through adopting parallel bimorphs, namely, through increasing the piezoelectric and dielectric coefficients, better actuation efficiency as well as better sensing capability is achieved.

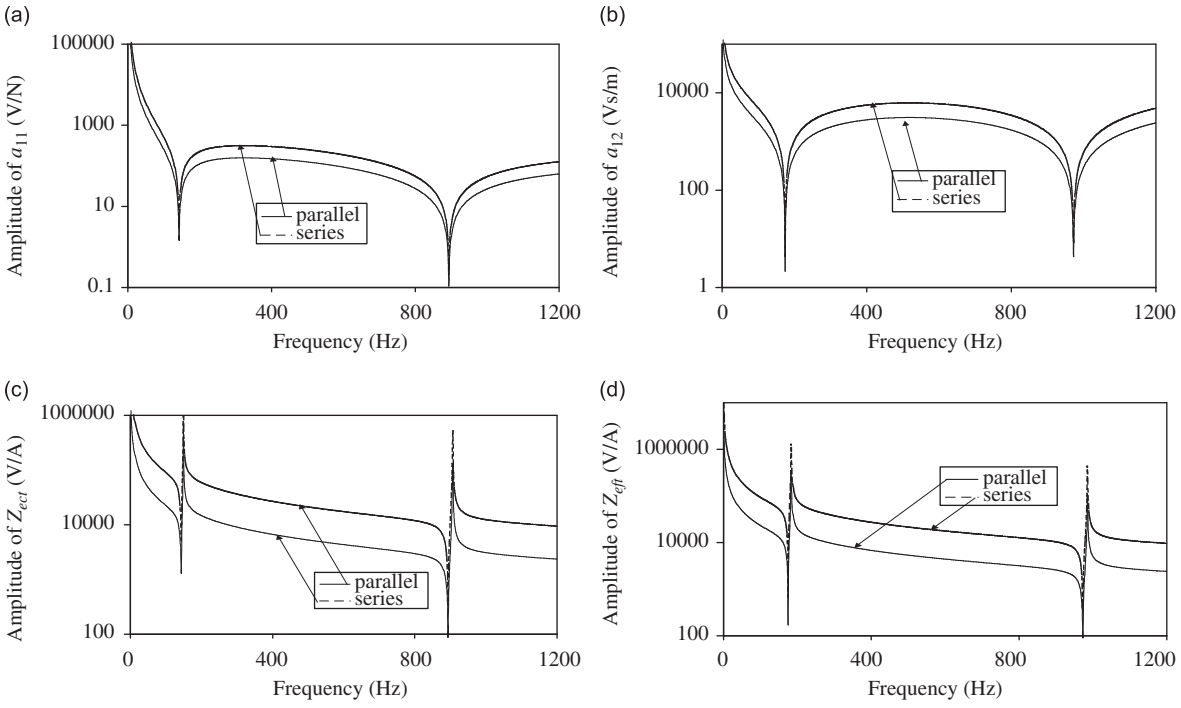

Fig. 8. Transduction/calibration functions of BITs with series or parallel type bimorphs: (a) a_{11}, (b) a_{12}, (c) Z^t_{ec}, and (d) Z^t_{ef}.

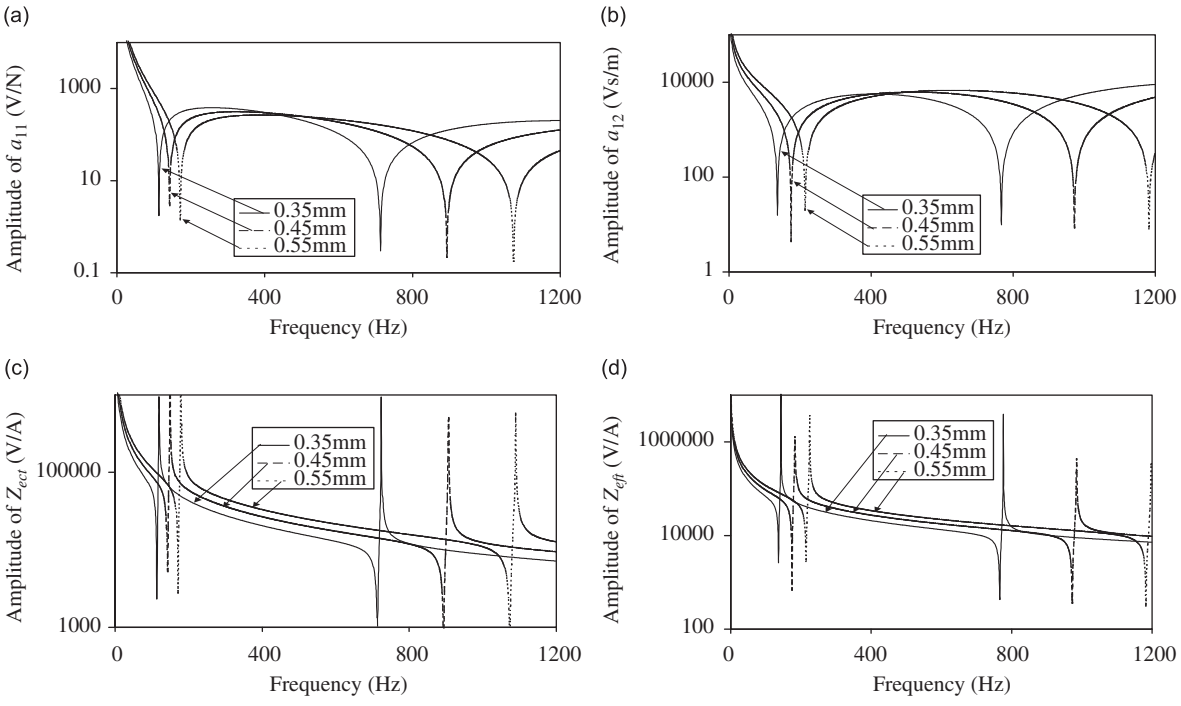

Fig. 9. Transduction/calibration functions of BITs with different bimorph thickness: (a) a_{11}, (b) a_{12}, (c) Z^t_{ec}, and (d) Z^t_{ef}.

From Fig. 9, it is observed that thicker bimorphs correspond to larger natural frequencies of all the functions. This conforms to the fact that the increase in bimorph thickness results in the increase in both stiffness and mass of the transducer, while the increase in stiffness has a larger effect on natural frequencies

than the increase in mass. For calibration functions Z^t_{ec} and Z^t_{ef}, PZT thickness not only affects their natural frequencies, but influences their amplitudes. Generally speaking, the thinner PZT layers result in smaller amplitudes of the electrical impedances and therefore improve the sensing capability of a BIT.

6. Conclusions

In this paper, a Bimorph Impedance Transducer is modeled and analytically characterized. The closed-form calibration functions ($Z^t_{ec}, Z^t_{ef}, Z^t_{MO}$) and transduction functions (a_{11}, a_{12}, a_{21}, a_{22}) are derived based on the piezoelectric constitutive equations and beam theory. With these closed-form formulae, the dynamic performance of a BIT under various boundary conditions is directly related to the physical parameters of the transducer itself. After the effectiveness of these formulae is verified by experiments, these formulae are utilized to improve the actuation and sensing performance of a BIT. Through two examples, in which different bimorph types (series versus parallel bimorph) and dimensions are employed for a BIT, it is found that it is feasible to design BITs with better actuation efficiency and sensing capability.

The analytical approach is of great importance for design and optimization of a Bimorph Impedance Transducer. For instance, miniaturization is one major trend in product design in recent years. To measure mechanical impedance of mini-structures, a suitable BIT has to be very small in size. Calibration of such a miniature transducer will pose difficulties in experiments, making the design and optimization a difficult job. However, with the analytical solutions, such work can be easily performed, saving considerable money and time. The BIT has been successfully employed to measure translational and rotational FRFs of elastic structures including one-dimensional beam and two-dimensional plate [15,16].

References

[1] P.L. Chen, R.S. Muller, R.D. Jolly, G.L. Halac, R.M. White, A.P. Andrews, T.C. Lim, M.E. Motamedi, Integrated silicon microbeam PI-EFT accelerometer, *IEEE Transactions on Electron Devices* ED-29 (1) (1982) 27–33.
[2] G. Caliano, N. Lamberti, A. Iula, M. Pappalardo, A piezoelectric bimorph static pressure sensor, *Sensors and Actuators A—Physical* 46 (1995) 176–178.
[3] J. Kelly Lee, Piezoelectric bimorph optical beam scanners: analysis and construction, *Applied Optics* 18 (4) (1979) 454–459.
[4] V.D. Kugel, B. Xu, Q.M. Zhang, L.E. Cross, Bimorph-based piezoelectric air acoustic transducer: model, *Sensors and Actuators A—Physical* 69 (1998) 234–242.
[5] P. Vairac, S. Ballandras, B. Cretin, Finite element analysis of the behavior of the scanning microdeformation microscope, *IEEE Transactions on Ultrasonics, Ferroelectrics, and Frequency Control* 48 (4) (2001) 895–899.
[6] C.J. Morris, F.K. Forster, Optimization of a circular piezoelectric bimorph for a micropump driver, *Journal of Micromechanics and Microengineering* 10 (2000) 459–465.
[7] G. Smits, S.I. Dalke, T.K. Cooney, The constituent equations of piezoelectric bimorphs, *Sensors and Actuators A—Physical* 28 (1991) 41–61.
[8] J.G. Smits, A. Ballato, Dynamic admittance matrix of piezoelectric cantilever bimorphs, *Journal of Microelectromechanical Systems* 3 (3) (1994) 105–112.
[9] J.G. Smits, A. Ballato, Dynamic behavior of piezoelectric bimorphs, *IEEE Ultrasonics Symposium* (1993) 463–465.
[10] A. Ballato, J.G. Smits, Simulation networks of piezobimorphs for robotic actuators, *IEEE Ultrasonics Symposium* 3 (1998) 1173–1176.
[11] Y.S. Cho, Y.E. Park, C.S. Han, S.K. Ha, Five-port equivalent electric circuit of piezoelectric bimorph beam, *Sensors and Actuators A—Physical* 84 (2000) 140–148.
[12] S.-F. Ling, Y. Xie, Monitoring structural integrity using a piezoceramic inertial actuator cum sensor, *Journal of Sound and Vibration* 247 (4) (2001) 731–737.
[13] S.-F. Ling, Y. Xie, Detecting mechanical impedance of structures using the sensing capability of a piezoceramic inertial actuator, *Sensors and Actuators A—Physical* 93 (3) (2001) 243–249.
[14] T. Ikeda, *Fundamentals of Piezoelectricity*, Oxford University Press, Oxford, 1990.
[15] X.Y. Hou, S.-F. Ling, K.H. Heng, A new transducer for detecting point impedance of structures to moment, *Proceedings of the 12th International Congress on Sound and Vibration ISCV*, Vol. 12, Lisbon, July 2005, pp. 11–14.
[16] X.Y. Hou, S.-F. Ling, K.H. Heng, Sensing translational impedance by a bimorph impedance transducer, *Sensors and Actuators A—Physical* 137 (2) (2007) 193–199.